

Chemical Modeling of the Capture of Radioiodine Species

September 2020

Neil J Henson
Michel Sassi
Andrew M Ritzmann
Scott Muller
Alyssa E. Johnson

DISCLAIMER

This report was prepared as an account of work sponsored by an agency of the United States Government. Neither the United States Government nor any agency thereof, nor Battelle Memorial Institute, nor any of their employees, makes **any warranty, express or implied, or assumes any legal liability or responsibility for the accuracy, completeness, or usefulness of any information, apparatus, product, or process disclosed, or represents that its use would not infringe privately owned rights**. Reference herein to any specific commercial product, process, or service by trade name, trademark, manufacturer, or otherwise does not necessarily constitute or imply its endorsement, recommendation, or favoring by the United States Government or any agency thereof, or Battelle Memorial Institute. The views and opinions of authors expressed herein do not necessarily state or reflect those of the United States Government or any agency thereof.

PACIFIC NORTHWEST NATIONAL LABORATORY
operated by
BATTELLE
for the
UNITED STATES DEPARTMENT OF ENERGY
under Contract DE-AC05-76RL01830

Printed in the United States of America

Available to DOE and DOE contractors from the
Office of Scientific and Technical Information,
P.O. Box 62, Oak Ridge, TN 37831-0062;
ph: (865) 576-8401
fax: (865) 576-5728
email: reports@adonis.osti.gov

Available to the public from the National Technical Information Service
5301 Shawnee Rd., Alexandria, VA 22312
ph: (800) 553-NTIS (6847)
email: orders@ntis.gov <<https://www.ntis.gov/about>>
Online ordering: <http://www.ntis.gov>

Chemical Modeling of the Capture of Radioiodine Species

September 2020

Neil J Henson
Michel Sassi
Andrew M Ritzmann
Scott Muller
Alyssa E Johnson

Prepared for
the U.S. Department of Energy
under Contract DE-AC05-76RL01830

Pacific Northwest National Laboratory
Richland, Washington 99354

1.0 Introduction

Iodine is a common fission product resulting from the transmutation of uranium fuel in nuclear power reactors. The short-lived radioactive isotope, ^{131}I , with a half-life of around eight days, would be a particular health concern if released into the environment. Capture materials, such as activated carbon, are used routinely in nuclear power plants^{1,2} and medical isotope production facilities³ to remove this hazard during normal operations to reduce emissions to acceptable levels. Iodine, unlike other common fission products such as noble gases, is challenging because of the wide range of molecular forms and oxidation states (from +VII in IF_7 to -I in iodide) that it displays, which can interconvert both in the gas phase and in the solution phase for example. In the atmosphere, a variety of chemical forms are observed due to radical pathways that can be initiated by interaction with light, whereas in the solution phase, iodide (I^-), iodate (IO_3^-) and molecular iodine (I_2) are the most common species. In the event of a nuclear incident and subsequent release of radioactive iodine, such as the Fukushima accident, iodine-containing species could potentially interact with a number of surfaces causing further molecular interconversions, including the stainless steel reactor vessel, soil in the sub-surface and particulates in the atmosphere. Consequently, a detailed understanding of these complex chemical networks is required to design effective emergency response to contain the hazard to human health. The foundational science needed as a basis for this understanding begins with simple models of how iodine-containing molecules interact with surfaces such as pristine graphite surfaces as surrogates for one of the most important components in an activated carbon material.

The work in this project is focused on three computational tasks. In the first, we consider the binding of iodine-containing molecules of varying oxidation states to the major component of activated carbon – pristine graphene-like sheets. The aim of this task was to verify that the main mode of interaction with the surface was through physisorption. The second task focused on molecular binding and possible chemical transformations resulting from the reaction of molecular iodine with chemical functional groups on the edge of the graphene sheets or surface defects in the sheet itself. Spectroscopy and elemental analysis has shown the presence of a small number of these groups and adsorption measurements indicate these sites may lead to irreversible adsorption of iodine likely from a chemisorption process. The exact nature of these effects at the atomic level is not known and this task was focused on investigating these processes. The final task was associated with radiolytic breakdown of ^{131}I to ^{131}Xe in iodine-containing molecules and investigated the resulting molecular fragmentation process both in the gas phase and on the graphene-like surface. For each of the tasks, the intent was to learn about the thermodynamics and kinetics of the chemical transformations and use the calculations to provide parameters for input into kinetic models describing these processes for interpretation of experimental data in future work.

2.0 Binding of Iodine-Containing Molecules to Graphene Sheets

2.1 Background

This task is focused on calculations of the binding of iodine-containing molecules to graphene surface models. To increase the sophistication of the models, we consider several layers of graphene in the model so that the sub-surface effects that would be present in graphite are included.

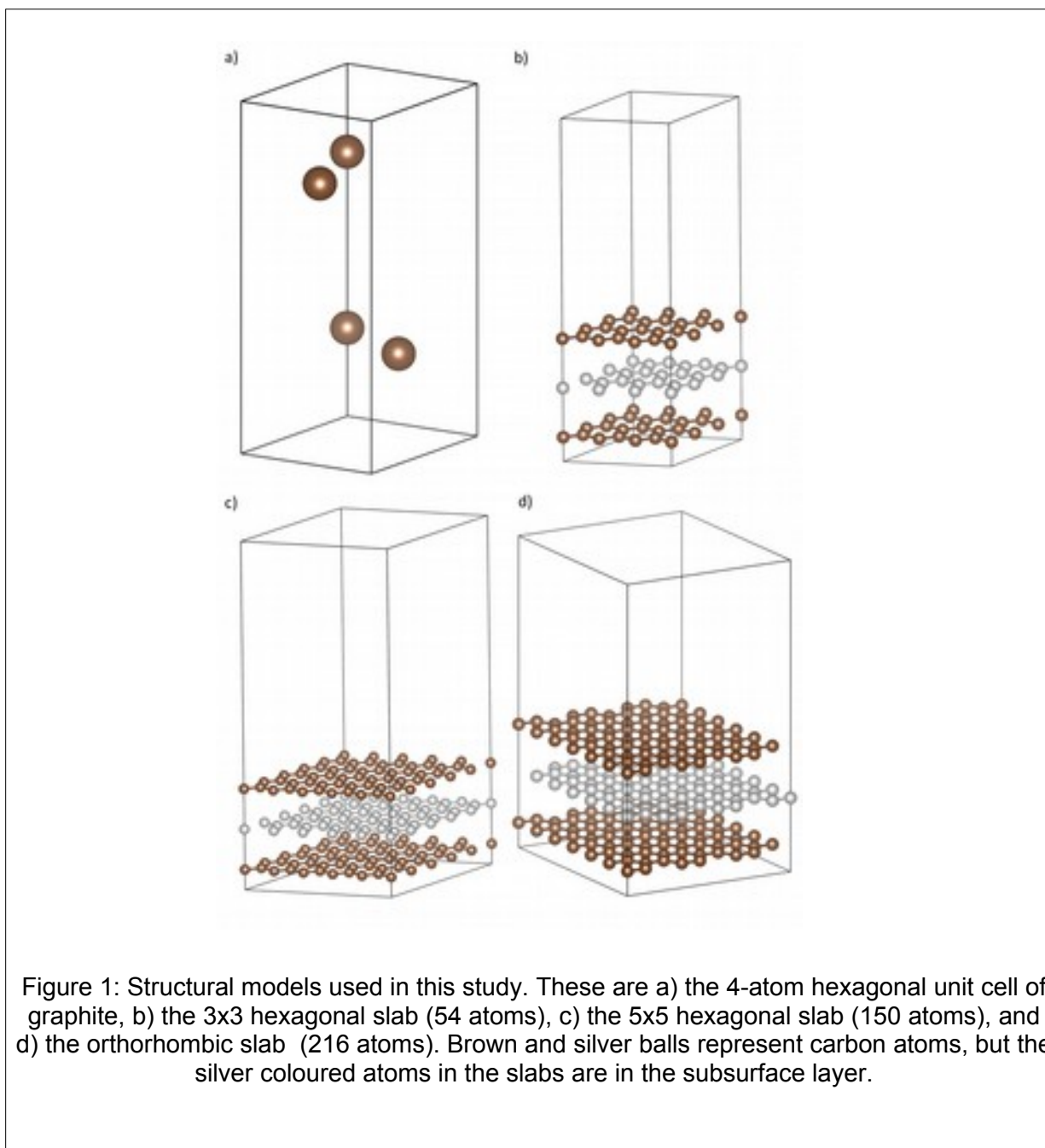
The interaction of iodine-containing species with carbon-based capture materials has been studied extensively both experimentally and theoretically with a focus on molecular iodine, I_2 . Measurements have been made to probe the adsorption and desorption behaviour on activated carbons⁴⁻⁸ and also other carbon materials such as graphite,^{9,10} coal¹¹ and carbon black.¹² Notably, Park and Yang⁸ determined the activation energy for desorption to be approximately 51 kJmol^{-1} , which is a direct measure of the strength of interaction between iodine and the sorbent. Salzano measured both physisorption and chemisorption during adsorption of iodine on graphite.⁹ Iwamoto and Oishi showed that both the heats of adsorption and activation energies for desorption varied with coverage for iodine on graphite.¹⁰ The heat of adsorption were reported as ranging from $50\text{-}79 \text{ kJmol}^{-1}$, whereas for the activation energy of desorption distinction was made between physisorbed iodine ($79\text{-}130 \text{ kJmol}^{-1}$) and chemisorbed iodine ($142\text{-}200 \text{ kJmol}^{-1}$). Kipling and co-workers make conclusions regarding the packing structure of molecular iodine on the carbon surface based on the measured adsorption capacity,¹² and related it to that observed in the molecular iodine crystal structure. Although direct structural observation of iodine on the carbon surface are difficult, spectroscopic probes can provide useful information. Ghosh and co-workers performed measurement of shifts in Raman bands on adsorption of halogen molecules on nanotubes and graphene, and correlated the observations with density functional theory calculations.¹³ They observed a relationship between the electronic structure perturbations and the electron affinities of the molecules.

The majority of the computational studies have focused on the behavior of molecular iodine bound to graphene surfaces. Gerber and co-workers studied the adsorption of both atomic and molecular iodine on graphene surfaces using a number of density functionals including non-local van der Waals corrections.¹⁴ The calculated adsorption energy is strongly dependent on the binding site geometry and spans a range of $30\text{-}50 \text{ kJmol}^{-1}$. Rudenko and co-workers investigated the binding of diatomic halogen molecules to graphene surfaces using a van der Waals density functional methods.¹⁵ They calculated binding energies ranging from $34\text{-}36 \text{ kJmol}^{-1}$ for out-of-plane geometries and $48\text{-}50 \text{ kJmol}^{-1}$ for in-plane geometries. They also predict the contribution of charge-transfer to the binding energy.

In this task, we present a comprehensive fundamental computational study addressing the interaction of a number of iodine-containing molecules with a graphite surface examining the effect of choice of modelling approach, system size and model representation to predict binding geometries and energetics. In particular, we probe the extent to which charge transfer may occur between the surface and the sorbed molecule to understand the balance between physisorption and chemisorption effects.

2.2 Methods and Models

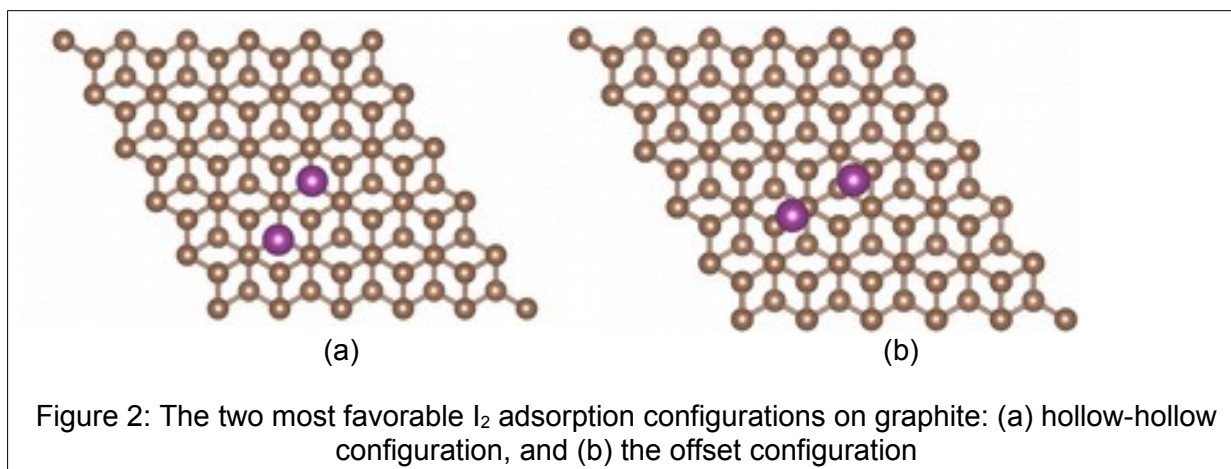
The graphite (0001) surface was employed as a surrogate model for the surface of activated carbon. The slab is shown in Figure 1. The exposed surface is a plane of sp^2 hybridized carbons corresponding to a single graphene layer. The slab model contains three layers with the middle layer offset from the top and bottom layers. This arises from the crystal structure of graphite, and it means that the central layer has carbons lying below the hexagon centers (hollow sites) and half of the carbon atom in the surface layers. Adopting an odd number of layers allows for the top and bottom layers to be aligned.



Spin-polarized Kohn-Sham density functional theory (KS-DFT)^{16,17} calculations were performed using the Vienna *ab Initio* Simulation Package (VASP) version 5.4.4.^{18–20} The projected augmented-wave method (PAW) was used to represent the interactions between nuclei and electrons.²¹ Standard (not soft) PAW potentials were taken from the VASP library²² with the following valence electrons treated explicitly: H (1s¹), C (2s²2p²), O (2s²2p⁴), and I (5s²5p⁵). Electron exchange-and-correlation (XC) was treated within the generalized gradient approximation (GGA) of Perdew, Burke, and Ernzerhof²³ (PBE) and the strongly constrained and appropriately normed (SCAN)²⁴ meta-GGA functionals. The plane-wave kinetic energy cutoff was 900 eV. For the hexagonal graphite unit cell, a 15 x 15 x 9 γ -centered mesh was used, and super-cell calculations were adjusted to keep the k-point spacing approximately constant. Gaussian smearing with a width of 0.1 eV was employed. This approach keeps the entropic contribution to the total energy below 1 meV/atom. With these parameters, the total energy of the graphite unit cell (4 atoms) was converged to 1 meV/atom. Bulk system band structures were computed using the improved tetrahedron method of Blöchl, Jepsen, and Andersen.²⁵ For slab calculations, only 1 k-point was used in the direction normal to the surface to minimize interactions between the slab and its periodic image. At least 10 Å of vacuum was placed between the slab and its periodic image.

Graphite contains carbon atoms covalently bonded in planes. The layers are held together through dispersion (van der Waals) interactions. GGA functionals such as PBE poorly describe dispersion as evidenced by the lack of adhesion between layers in graphite. It is expected that meta-GGA functionals should incorporate some intermediate-range dispersion interactions.²⁶ However, several methods have been proposed to correct for this behavior. These fall into two classes: *a posteriori* corrections that depend on an empirical potential (for example, Grimme's DFT-D family of corrections)²⁷ and self-consistent corrections where an explicit dispersion term is added to the XC functional (for example, the DFT-DF approach).²⁸ In this work, we employ Grimme's DFT-D3 approach to dispersion interaction.

2.3 Results

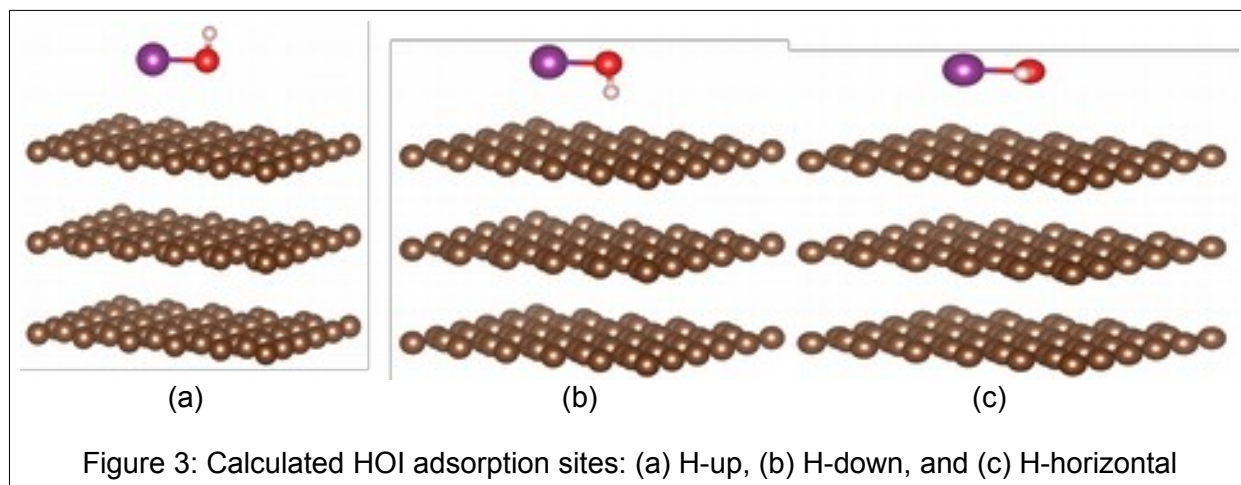


The analysis of I₂ adsorption on graphite requires considering the structure of the graphite (0001) surface. The 3x3 surface slab was used for an initial survey of the potential sites where molecular iodine could adsorb. High-symmetry sites were used to anchor the first iodine atom, and the second was placed either directly above the first atom or over another high symmetry

site with the I_2 molecule angled upward from the first atom to the second atom. This initial geometry search revealed that the most favorable conformation was placing the I_2 parallel to the surface. Furthermore, two configurations had the strongest adsorption energies (Figure 2). The first configuration involves the iodine atoms each sitting above a hollow site. The second configuration has one iodine displaced from the hollow site toward a top site while the second iodine resides on (or near) a bridge site. The adsorption energies computed with the PBE-D3 methodology are 33.1 and 32.4 kJ/mol, respectively. Pure PBE calculations for the hollow-hollow configuration give a binding energy of less than 1 kJ/mol. This indicates that surface- I_2 interaction is almost all dispersive.

The simplest non-diatomic molecule containing iodine is hypoiodous acid, HOI. This species is frequently discussed in the context of molecular iodine dissolving into aqueous solutions.²⁹ However, it is a likely species in a nuclear reactor effluent.¹ The HOI molecule is bent which adds numerous adsorption configurations. Namely, does the molecule lie flat, or at an perpendicular to the surface? What atom prefers to be closest to the surface, and where is the molecule positioned relative carbons in the surface layer?

To answer these questions, we start with three possible configurations of the HOI molecule featuring the I-O bond parallel to the surface and the O-H bond directing the H atom toward the surface (down), parallel to the surface (flat), or away from the surface (up) as shown in Figure 3. These configurations are augmented by placing the iodine above the high-symmetry sites (hollow, top, bridge) and rotating the molecule such that the I-O bond is directed toward an adjacent high symmetry site though the O will not lie directly on top of that site. Optimization of the initial configurations using the PBE-D3 approach reveals that the flat configuration is not stable and results in the hydrogen rotating into the down configuration.



After optimization, the strongest adsorption occurs with the iodine on a hollow site and the oxygen sitting on a bridge site with the I-O bond crossing a top site. The hydrogen is pointing down. Ultimately, adsorption in this configuration is favorable by 30.8 kJ/mol. The complete set of adsorption results shows that the iodine prefers the hollow site by approximately 6 kJ/mol and that having the hydrogen point toward the surface is preferable by 5-6 kJ/mol. The surface-iodine distance is comparable to the adsorption of I_2 *vide supra* which leaves plenty of space for the oxygen and the hydrogen to move toward the surface. This adds favorable dispersion interactions with the surface resulting in a lower adsorption energy. The most favorable configuration suggests that monolayer adsorption of HOI would involve one molecule per hollow site.

A Bader charge analysis of the HOI molecule shows that no charge transfer occurs upon adsorption. This is not unexpected, however, since the electron density arises from a DFT-PBE calculation which fails to properly describe dispersion interactions. Thus, no significant perturbation happens to the HOI molecule when it adsorbs to the surface.

3.0 Binding of molecular iodine to edge sites

3.1 Background

Activated carbon (AC) is a sorbent material that has been utilized in capturing radioactive contaminants, including ^{131}I . However, the mechanisms for AC's capture of iodine are not well understood— for example, AC has edge groups and chemistry that can vary depending on its source³⁰ and the treatments it has undergone.^{31–35} It is also unknown to what extent iodine may be chemisorbed (adsorbed via chemical reactions) vs. physisorbed when captured by AC. However, if chemisorption is to occur, it will most likely happen near functional groups at AC edges which are chiefly responsible for AC's surface chemistry.³¹ We used first principles calculations to predict whether chemisorption of iodine is energetically favorable at common AC edge sites. It is unfeasible to represent the complex structure of AC at this scale, so we use graphene nanoribbons and flakes as surrogates for AC, as shown in Figure 4. Oxygen is the main non-carbon species present in AC, and is responsible for much of its chemistry,³¹ so we focus on simple functional groups that contain oxygen, including phenol and carboxyl groups.

3.2 Methods and Models

To model graphene nanoribbons we performed DFT calculations using VASP,^{18,20,36} while *ab initio* calculations were implemented for graphene flakes using NWChem.³⁷ We quantified the energetic favorability of iodine chemisorption at an edge site by computing the reaction energy (heat of formation) by the simple equation

$$\Delta E_{\text{reaction}} = \sum E_{\text{products}} - \sum E_{\text{reactants}},$$

where a negative value indicates that the reaction is favorable (exothermic), and a positive value indicates the reaction is unfavorable (endothermic).

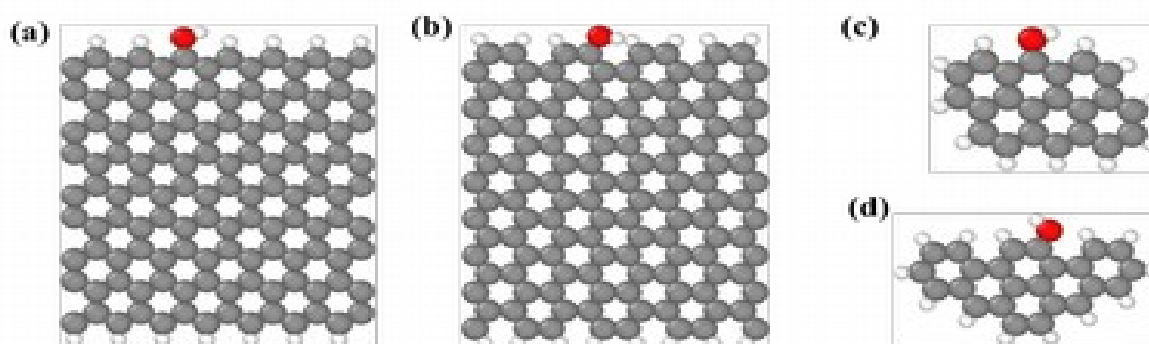


Figure 4: Surrogates for activated carbon (AC) edges, with phenol functional group shown as an example. AC is represented by either graphene nanoribbons (a-b), or graphene flakes (c-d), with either zigzag (a, c) or armchair (b, d) edges.

3.3 Results

The chemisorption reaction energies of the iodine species I_2 and HI at pristine edges and at phenol edge groups are listed in Table 1. Results from NWChem and VASP were in reasonably good agreement despite the difference in their structure (flake and nanoribbon respectively). We found that zigzag edges tended to be more energetically favorable than armchair edges. However, in all cases we found iodine chemisorption to be highly endothermic and therefore unfavorable. This is especially true when oxygen is present. The other edge groups we tested yielded similar results, indicating that chemisorption is unlikely to occur at either pristine edges or at oxygen-based functional group sites. This is surprising as there is evidence that iodine chemisorption into activated carbon can and does occur. We are currently investigating different routes to chemisorption, including through epoxide groups which are present in graphene oxide and that may facilitate iodine chemisorption, or via other elements such as potassium that may serve as catalysts.

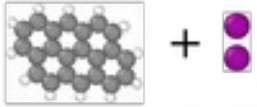
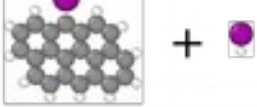
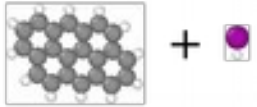
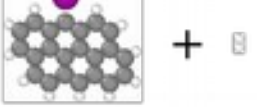
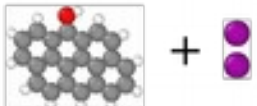
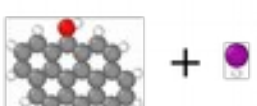
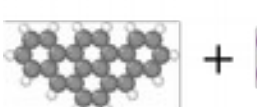
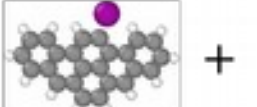
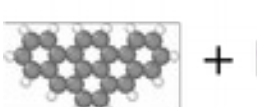
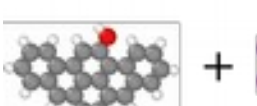
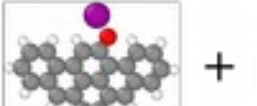
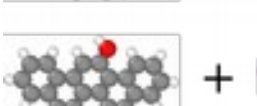
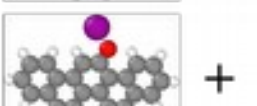
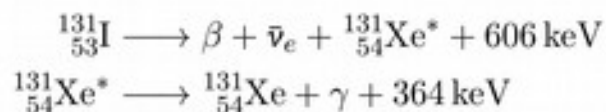
<u>Reactant</u>	<u>Product</u>	$\Delta E_{\text{reaction}}$ (kcal/mol)	
		<u>NWChem</u>	<u>VASP</u>
		+61	+69
		89	+80
		+136	unstable
		+172	unstable
		+91	+93
		+119	+104
		+161	+148
		+189	+159

Table 1: Predicted reaction energies for chemisorption of iodine species on pristine edge or phenol edge group. Graphene flake images are shown in the table to represent the given reaction, but note that VASP calculations use nanoribbons as shown in Figure 1(a-b). Carbon atoms are grey, hydrogen atoms are white, oxygen atoms are red, and iodine atoms are purple.

4.0 Transmutation of radioiodine containing molecules

4.1 Background

I₂ and CH₃I can be generated in the upper ocean layers and migrate the atmosphere.³⁸ Photolysis and ozonolysis reactions convert these species into iodine oxides (IO_x) and acidic iodine (HIO_x) species,^{39–41} generating a wide array of iodine-containing chemical species in the atmosphere with a large number of oxidation states possible, ranging from –I to +V. In the case of radioiodine, this complex iodine chemistry is further complicated by the short a half-life of ¹³¹I, about 8 days,⁴² after which it undergoes β-decay leading to the creation of ¹³¹Xe and the emission of an anti-neutrino ($\bar{\nu}_e$), a β⁻ particle, and γ-rays:



Upon decay, ¹³¹I releases a total of 970 keV of energy in a two-step process. The first step involves the emission of β-particles having a maximum kinetic energy of 806.9 keV, followed by the emission of γ-rays with a most probable energy of 364 keV. At the end of the decay process, a stable daughter ¹³¹Xe isotope is created. While the β-particles can travel up to 0.2 cm away in water⁴³ from the ¹³¹Xe nucleus, the physical and chemical changes induced by the transmuted ¹³¹Xe have effects on the nanometer scale. In a molecular context, the local perturbations imposed by ¹³¹I transmutation at first seem insurmountable as four different atomic-scale disruptions arise: (i) the abrupt appearance of a xenon nucleus, (ii) the creation of a positively charged Xe ion isoelectronic with its parent, (iii) potential additional ionizations due to the reorganization of the electron cloud adjusting from ¹³¹I to ¹³¹Xe⁺ nucleus (a process also referred as electron shake-off⁴⁴), and (iv) a physical recoil of the daughter Xe nucleus, in which a certain amount of kinetic energy is given to Xe in accordance with momentum conservation between the energy released during radioactive decay and the products of the reaction. Altogether, these effects have the potential to break bonds and create new chemical environments which could potentially alter the properties of capture materials.

4.2 Methods and Models

The Vienna *ab Initio* Simulation Package (VASP) package¹³ has been used to perform AIMD modeling of bond breaking events in molecules after ¹³¹I transmutation. The generalized gradient approximation (GGA) exchange-correlation functional, as parametrized by Perdew-Burke-Ernzerhof,¹⁴ with the Grimme¹⁵ dispersion corrections (i.e., PBE+D3) has been used in all the simulations. The PAW potentials for H, C, O, I, and Xe respectively used a valence electronic configuration of 1s¹, 2s² 2p², 2s² 2p⁴, 5s² 5p⁵, and 5s² 5p⁶. The simulations were performed in the NVE ensemble with a 0.1 fs time step and an electronic self-consistent field energy convergence criterion of 10⁻⁶ eV/cell. To correctly describe bond breaking events, spin-

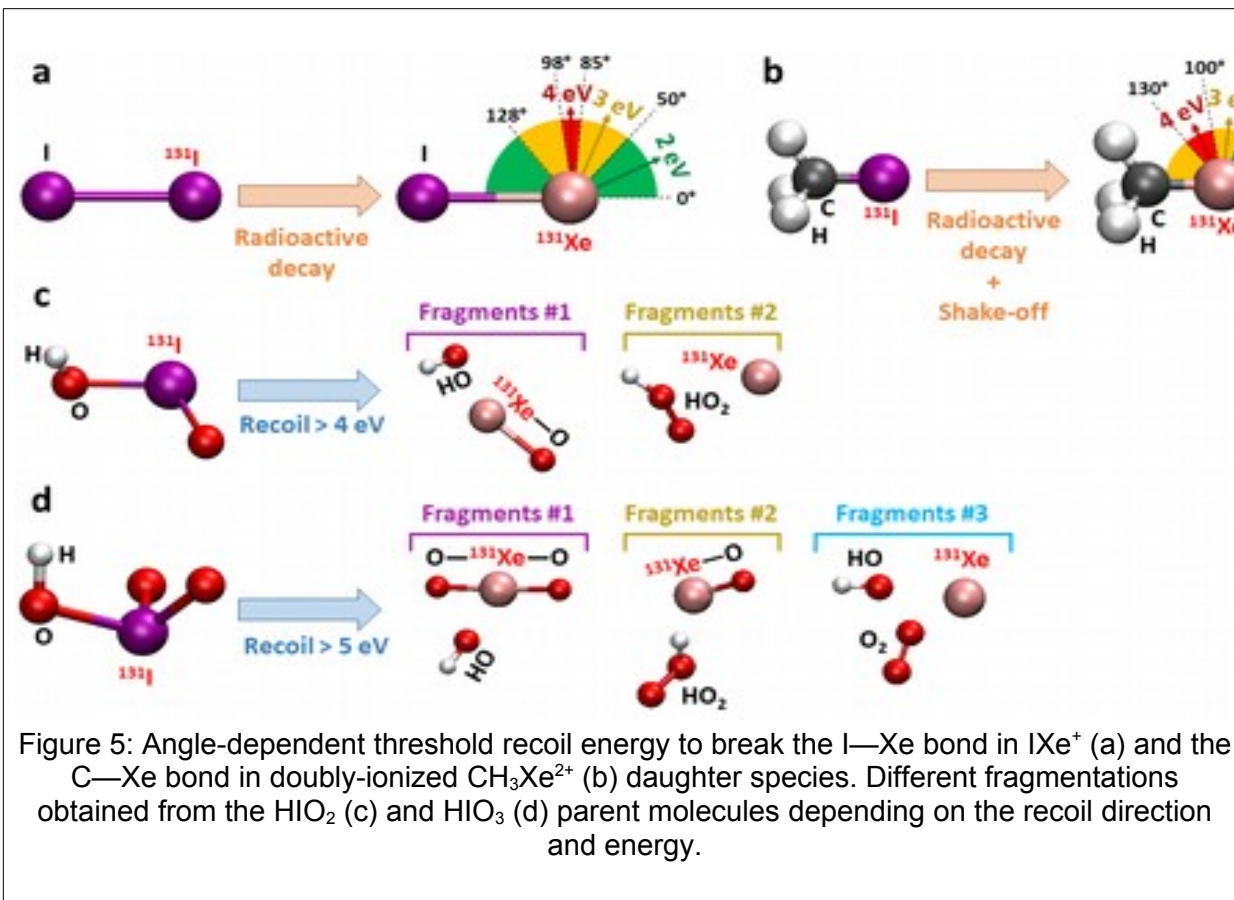
polarization was used. Bond breaking was detected by monitoring the time-evolution distance between the recoiling atom and the other atoms constituting the molecule.¹⁶ The simulations of $^{131}\text{Xe}^+$ recoil in gas phase molecules used a cubic cell of 15 Å in each of the three cartesian directions, only the Γ -point was used to sample the Brillouin zone, and a plane-wave basis set cutoff of 400 eV. The simulations of $^{131}\text{Xe}^+$ recoil in radioiodine-containing molecules adsorbed on graphite used a hexagonal supercell size of $a=b=19.73$ Å, and $c=27.0$ Å, and a three-layers graphite slab with exposed (0001) facets. A three-layers slab was used because it allows to have a slab with symmetric top- and bottom-surfaces while providing an offset subsurface layer representative of the graphite structure.

Modeling of the ^{131}I transmutation event in the radioiodine-containing molecules I_2 , HI, HIO, HIO_2 , HIO_3 , and CH_3I has been performed using *ab initio* molecular dynamics simulations. To mimic the physical and chemical consequences of ^{131}I radioactive decay, such as the emission of a β -particle leading to an ionization of the daughter nucleus (i.e. $^{131}\text{Xe}^+$) and the physical recoil of $^{131}\text{Xe}^+$, we removed one electron from the system and attributed an initial kinetic energy to the $^{131}\text{Xe}^+$ species. In the simulations, a jellium background has been used to compensate for the loss of charge. To explore the effects of ^{131}I transmutation on the molecular stability, we performed a series of AIMD simulations in which the $^{131}\text{Xe}^+$ recoils in different directions. Further, for each direction investigated, a series of simulations was carried out with a different initial kinetic energy for the recoiling $^{131}\text{Xe}^+$ species. Because an exhaustive exploration of all the possible recoil directions for a given molecule would require a considerable amount of simulation time, we have chosen to limit our investigations to directions aligned with the bonds in the molecules. This implies that the determined recoil threshold energy for bond breaking obtained is a lower limit of the recoil required to typically break a bond. This concept has been illustrated in the case of the I_2 and CH_3I molecules for which the daughter $^{131}\text{Xe}^+$ recoil has been initiated at different angles with respect to the molecular bond axis.

4.3 Results

Ab initio molecular dynamic simulations have been performed to identify the possible fragmentation products of radioiodine-containing molecules of I_2 , HI, HIO, HIO_2 , HIO_3 , and CH_3I after for ^{131}I decay in both the gas phase (Figure 5) and adsorbed on a graphite surface. Gas phase calculations found that I_2 is the least resistant to radiolytic fragmentation, requiring 2 eV of recoil for decomposition. The HIO_x family of molecules is found to be more resilient than I_2 , with a bond breaking threshold recoil energy of more than 4 eV, while HI and CH_3I molecules do not fragment after ^{131}I transmutation. Accounting for electron shake-off in methyl iodide has shown that fragmentation occurs for the doubly-ionized daughter molecule (Figure 5). Simulations of transmutation in radioiodine-containing molecules adsorbed on graphite showed that the threshold recoil energy leading to bond breaking is considerably lowered. While the identification of gas phase fragments can offer a new chemical route to consider in chemical kinetics models, we found that the formation of reactive fragment products at the graphite surface can favor their reaction with surface carbon atoms. Especially, the CH_3 and OH radicals are found to form covalent bonds with graphite which over time could potentially play a role in

reducing the number of adsorption sites of capture materials available, and hence, negatively impact their capture capability.



5.0 Conclusion

Electronic structure calculations have been used to determine the structure and binding energies of iodine-containing molecules to different structural components for activated carbon, including graphene-like structural elements and chemical functional groups on the edge of graphene sheets. It is predicted that the molecules bind only weakly to graphene-like surfaces with the dominant interactions being dispersive in nature consistent with physisorption. However, chemical reactions are possible with edge-bound functional group, although they are predicted to be endothermic in nature when those groups contain oxygen.

Ab initio molecular dynamic simulations have been used to identify the possible fragmentation products of radioiodine-containing molecules in both the gas phase and adsorbed on a graphite surface. Gas phase calculations found that I_2 is the least resistant to radiolytic fragmentation, requiring 2 eV of recoil for decomposition. The HIO_x family of molecules is found to be more resilient than I_2 , with a bond breaking threshold recoil energy of more than 4 eV, while HI and CH_3I molecules do not fragment after ^{131}I transmutation. Accounting for electron shake-off in methyl iodide has shown that fragmentation occurs for the doubly-ionized daughter molecule. Simulations of transmutation in radioiodine-containing molecules adsorbed on graphite showed that the threshold recoil energy leading to bond breaking is considerably lowered. While the identification of gas phase fragments can offer a new chemical route to consider in chemical kinetics models, we found that the formation of reactive fragment products at the graphite surface can favor their reaction with surface carbon atoms. Especially, the CH_3 and OH radicals are found to form covalent bonds with graphite which over time could potentially play a role in reducing the number of adsorption sites of capture materials available, and hence, negatively impact their capture capability.

6.0 Acknowledgements

This research was supported by the Laboratory Directed Research and Development (LDRD) and Chemical Dynamic Initiative (CDI) at Pacific Northwest National Laboratory (PNNL). PNNL is a multi-program national laboratory operated by Battelle for the U.S. Department of Energy. Computational resources were provided by PNNL Institutional Computing (PIC).

7.0 Bibliography

1. Riley, B. J., Vienna, J. D., Strachan, D. M., McCloy, J. S. & Jerden, J. L. Materials and Processes for the Effective Capture and Immobilization of Radioiodine: A Review. *J Nucl Mater* **470**, 307–326 (2016).
2. Vellingiri, K., Kim, K.-H., Pournara, A. & Deep, A. Towards High-Efficiency Sorptive Capture of Radionuclides in Solution and Gas. *Prog. Mater. Sci.* **94**, 1–67 (2018).
3. Doll, C. G. *et al.* Abatement of Xenon and Iodine Emissions From Medical Isotope Production Facilities. *J. Environ. Radioact.* **130**, 33–43 (2014).
4. Reyerson, L. H. & Cameron, A. E. The Sorption of Bromine and Iodine by Activated Charcoal. *J. Phys. Chem.* **40**, 233–237 (1936).
5. Juhola, A. J. Iodine adsorption and structure of activated carbons. *Carbon* **13**, 437–442 (1975).
6. Liu, D., Zhao, J., Sung, C. & Zhang, L. The desorption isotherms of iodine from the catalyst of iodine-activated carbon. *Carbon* **31**, 81–85 (1993).
7. Bhatia, S. K., Liu, F. & Arvind, G. Effect of Pore Blockage on Adsorption Isotherms and Dynamics: Anomalous Adsorption of Iodine on Activated Carbon. *Langmuir* **16**, 4001–4008 (2000).
8. Park, J.-H. & Yang, R. T. Predicting Adsorption Isotherms of Low-Volatile Compounds By Temperature Programmed Desorption: Iodine on Carbon. *Langmuir* **21**, 5055–5060 (2005).
9. Salzano, F. J. The behavior of iodine in graphite. *Carbon* **2**, 73–81 (1964).
10. Iwamoto, K. & Oishi, J. The Behavior of Iodine in Adsorption and Desorption by Graphite. *J. Nucl. Sci. Technol.* **5**, 437–446 (1968).
11. Aronson, S., Schwebel, A. & Sinensky, G. Absorption of iodine by coal and lignite. *Carbon* **14**, 93–95 (1976).

12. Kipling, J. J., Sherwood, J. N. & Shooter, P. V. Adsorption of iodine from organic solvents by “graphitized” carbon blacks. *Trans Faraday Soc* **60**, 401–411 (1964).
13. Ghosh, S., Yamijala, S. R. K. C. S., Pati, S. K. & Rao, C. N. R. The interaction of halogen molecules with SWNTs and graphene. *RSC Adv* **2**, 1181–1188 (2012).
14. Tristant, D., Puech, P. & Gerber, I. C. Theoretical Study of Graphene Doping Mechanism By Iodine Molecules. *J. Phys. Chem. C* **119**, 12071–12078 (2015).
15. Rudenko, A. N., Keil, F. J., Katsnelson, M. I. & Lichtenstein, A. I. Adsorption of Diatomic Halogen Molecules on Graphene: a Van Der Waals Density Functional Study. *Phys. Rev. B* **82**, 035427–035427 (2010).
16. Hohenberg, P. & Kohn, W. Inhomogeneous Electron Gas. *Phys. Rev.* **136**, B864–B871–B864–B871 (1964).
17. Kohn, W. & Sham, L. J. Self-Consistent Equations Including Exchange and Correlation Effects. *Phys. Rev.* **140**, A1133–A1138–A1133–A1138 (1965).
18. Kresse, G. & Hafner, J. *Ab Initio* molecular Dynamics for Liquid Metals. *Phys Rev B* **47**, 558–561 (1993).
19. Kresse, G. & Furthmüller, J. Efficient Iterative Schemes Forab Initiototal-Energy Calculations Using a Plane-Wave Basis Set. *Phys. Rev. B* **54**, 11169–11186 (1996).
20. Kresse, G. & Furthmüller, J. Efficiency of ab-initio total energy calculations for metals and semiconductors using a plane-wave basis set. *Comput. Mater. Sci.* **6**, 15–50–15–50 (1996).
21. Blöchl, P. E. Projector augmented-wave method. *Phys. Rev. B* **50**, 17953–17979–17953–17979 (1994).
22. Kresse, G. & Joubert, D. From Ultrasoft Pseudopotentials To the Projector Augmented-Wave Method. *Phys. Rev. B* **59**, 1758–1775 (1999).
23. Perdew, J. P., Burke, K. & Ernzerhof, M. Generalized Gradient Approximation Made Simple. *Phys. Rev. Lett.* **77**, 3865–3868–3865–3868 (1996).

24. Sun, J., Ruzsinszky, A. & Perdew, J. P. Strongly Constrained and Appropriately Normed Semilocal Density Functional. *Phys. Rev. Lett.* **115**, 036402–036402 (2015).
25. Blöchl, P. E., Jepsen, O. & Andersen, O. K. Improved tetrahedron method for Brillouin-zone integrations. *Phys. Rev. B* **49**, 16223–16233–16223–16233 (1994).
26. Peng, H., Yang, Z.-H., Perdew, J. P. & Sun, J. Versatile van der Waals Density Functional Based on a Meta-Generalized Gradient Approximation. *Phys Rev X* **6**, 041005–041005 (2016).
27. Grimme, S., Antony, J., Ehrlich, S. & Krieg, H. A Consistent and Accurate *ab initio* Parametrization of Density Functional Dispersion Correction (DFT-D) for the 94 Elements H–Pu. *J Chem Phys* **132**, 154104–154104 (2010).
28. Lee, K., Murray, É. D., Kong, L., Lundqvist, B. I. & Langreth, D. C. Higher-accuracy van der Waals density functional. *Phys. Rev. B* **82**, 081101 (2010).
29. Bruchertseifer, H., Cripps, R., Guentay, S. & Jaeckel, B. Analysis of Iodine Species in Aqueous Solutions. *Anal. Bioanal. Chem.* **375**, 1107–1110 (2003).
30. Wang, Y. *et al.* Effect of Structural Defects on Activated Carbon Catalysts in Catalytic Wet Peroxide Oxidation of M-Cresol. *Catal. Today* **258**, 120–131 (2015).
31. Matheus, P., Carvahlo, J. & Guedes, D. Surface Modifications of Activated Carbon and Its Impact on Application. *Surf. Rev. Lett.* **26**, 1830006–1830006 (2019).
32. Bowling, R., Packard, R. T. & McCreery, R. L. Mechanism of Electrochemical Activation of Carbon Electrodes: Role of Graphite Lattice Defects. *Langmuir* **5**, 683–688 (1989).
33. Foo, G. S. & Sievers, C. Synergistic Effect Between Defect Sites and Functional Groups on the Hydrolysis of Cellulose Over Activated Carbon. *ChemSusChem* **8**, 534–543 (2014).
34. Yan, X. *et al.* Activated Carbon Becomes Active for Oxygen Reduction and Hydrogen Evolution Reactions. *Chem. Commun.* **52**, 8156–8159 (2016).
35. Yan, X., Jia, Y., Chen, J., Zhu, Z. & Yao, X. Defective-Activated-Carbon-Supported Mn–Co Nanoparticles As a Highly Efficient Electrocatalyst for Oxygen Reduction. *Adv. Mater.* **28**, 8771–8778 (2016).

36. Kresse, G. & Hafner, J. Ab Initio Molecular-Dynamics Simulation of the Liquid-Metal-Amorphous-Semiconductor Transition in Germanium. *Phys Rev B* **49**, 14251–14269 (1994).
37. Valiev, M. *et al.* NWChem: A Comprehensive and Scalable Open-Source Solution for Large Scale Molecular Simulations. *Comput Phys Commun* **181**, 1477–1489 (2010).
38. O'Dowd, C. D. & Hoffmann, T. Coastal New Particle Formation: a Review of the Current State-Of-The-Art. *Environ. Chem.* **2**, 245–245 (2005).
39. Bosland, L., Funke, F., Langrock, G. & Girault, N. Paris Project: Radiolytic Oxidation of Molecular Iodine in Containment During a Nuclear Reactor Severe Accident: Part 2. Formation and Destruction of Iodine Oxides Compounds Under Irradiation - Experimental Results Modelling. *Nucl. Eng. Des.* **241**, 4026–4044 (2011).
40. Khanniche, S., Louis, F., Cantrel, L. & Černušák, I. Thermochemistry of HIO₂ Species and Reactivity of Iodous Acid with OH Radical: A Computational Study. *ACS Earth Space Chem.* **1**, 39–49 (2017).
41. Dickinson, S. *et al.* Experimental and Modelling Studies of Iodine Oxide Formation and Aerosol Behaviour Relevant To Nuclear Reactor Accidents. *Ann. Nucl. Energy* **74**, 200–207 (2014).
42. Khazov, Y. A. Nuclear Data Sheets for a = 131. *Nucl. Data Sheets* **107**, 2715–2930 (2006).
43. Berger, M. J., Coursey, J. S., Zucker, M. A. & Chang, J. Stopping-Power & Range Tables for Electrons, Protons, and Helium Ions. *NIST Stand. Ref. Database* **124**, (2017).
44. Carlson, T. A., Nestor, C. W., Tucker, T. C. & Malik, F. B. Calculation of Electron Shake-Off for Elements From Z=2 to 92 With the Use of Self-Consistent-Field Wave Functions. *Phys. Rev.* **169**, 27–36 (1968).

Pacific Northwest National Laboratory

902 Battelle Boulevard
P.O. Box 999
Richland, WA 99354
1-888-375-PNNL (7665)

www.pnnl.gov